Resonance effects in correlated multilayer heterostructures

Irakli Titvinidze,* Antonius Dorda, Wolfgang von der Linden, and Enrico Arrigoni
Institute of Theoretical and Computational Physics, Graz University of Technology, 8010 Graz, Austria
(Received 22 July 2016; revised manuscript received 7 December 2016; published 27 December 2016)

We study the occurrence of negative differential conductance induced by resonance effects in a model for a multilayer heterostructure. In particular, we consider a system consisting of several correlated and noncorrelated monatomic layers sandwiched between two metallic leads. The geometry confines electrons in wells within the heterostructures, which are connected to each other and to the leads by tunneling processes. The nonequilibrium situation is produced by applying a bias voltage to the leads. Our results show that, for specific values of the parameters, resonance tunneling takes place. We investigate in detail its influence on the current-voltage characteristics. Our results are obtained via nonequilibrium real-space dynamical mean-field theory. As an impurity solver we use the so-called auxiliary master equation approach, which addresses the impurity problem within an auxiliary system consisting of a correlated impurity, a small number of uncorrelated bath sites, and two Markovian environments described by a generalized master equation.

DOI: 10.1103/PhysRevB.94.245142

I. INTRODUCTION

Quantum-mechanical resonance effects play an important role in physics and technology. A well-known example is resonant tunneling through potential barriers. Tunneling through two barriers, which becomes resonant at a specific external bias voltage, underlies the functioning of resonant tunneling diodes. Their applications range from high-speed microwave systems to novel digital logic circuits. Resonant tunneling through potential barriers is interesting from the theoretical point of view as well. To investigate this effect, one usually considers double- or multiwell structures made of semiconductor [1–4] or hybrid superconductor-semiconductor [5] materials, graphene [6–9] and graphene-boron [10–16] heterostructures. Different approaches are used to theoretically investigate their properties. One can mention, for example, the modified optical Bloch equations [3], self-consistent nonequilibrium Green's functions [4,17], the envelope wave-function formalism [17], adiabatic approximations [18], combinations of quantum transport random matrix theory with Bogoliubov-de Gennes equations [5], first-principle density functional theory [12], Bardeen transfer Hamiltonian approach [9], Wentzel–Kramers–Brillouin [6], and Lorentzian approximation for the quasiparticle spectral function [10]. However, to our knowledge, effects of electron correlations on resonant tunneling have so far been either neglected or included in a perturbative or mean-field way only. Here, we present a first study which examines the effect of correlations on resonant tunneling in an accurate and nonperturbative manner.

Recent experimental progress makes it possible to fabricate correlated heterostructures [19–24] with atomic resolution and, in particular, growing atomically abrupt layers with different electronic structures [20–22]. Here, we study a system which is composed of alternating strongly correlated and noncorrelated metallic layers, as well as band-insulator layers (see Fig. 1). The geometry of the system is such that electrons are confined in three wells connected by tunneling. The nonequilibrium situation is driven by applying a bias voltage to the leads, which introduces a homogeneous electric field in the central region. Resonant tunneling is mainly induced by the particular geometry, rather than the specific values of the system parameters. Since our goal is to investigate the qualitative behavior of this effect, we mainly perform calculations for one representative set of model parameters. In addition, in order to address the effect of correlations on resonance tunneling, we also investigate the behavior of the resonance current as a function of the interaction U.

In contrast to the previous works mentioned above, we use dynamical mean-field theory (DMFT) [25–27], which can treat electron-electron correlations accurately and is one of the most powerful methods to investigate high-dimensional correlated systems. Originally, DMFT was developed to treat equilibrium situations, and later extended [28–38] to the nonequilibrium case. This is formulated within the nonequilibrium Green's function approach originating from the works of Kubo [39], Schwinger [40], Kadanoff, Baym [41,42], and Keldysh [43].

DMFT is a comprehensive, thermodynamically consistent and nonperturbative scheme which becomes exact in infinite dimensions but usually quite well describes two- and three-dimensional systems. The only approximation in DMFT is locality of the self-energy. The latter can be calculated by mapping the original problem onto a single impurity Anderson model (SIAM) [44], whose parameters are determined self-consistently. For homogeneous systems the self-energies are the same for each lattice site due to translational symmetry, and, therefore, one needs to solve only one SIAM problem. For systems with broken translational invariance, as in the present case, the self-energies depend on the layer index z. Therefore, it is necessary to generalize the formalism and take into account the spatial inhomogeneity of the system [34,35,45–78] and, accordingly, to solve several SIAM problems.

In the present work the nonequilibrium SIAM problem is treated by using a recently developed auxiliary master equation approach [36,37,79], which treats the impurity problem within an auxiliary system consisting of a correlated impurity, a small number of uncorrelated bath sites, and two Markovian environments described by a generalized master equation.

The paper is organized as follows: Section II introduces the Hamiltonian of the system. In Sec. III we illustrate the

*irakli.titvinidze@tugraz.at

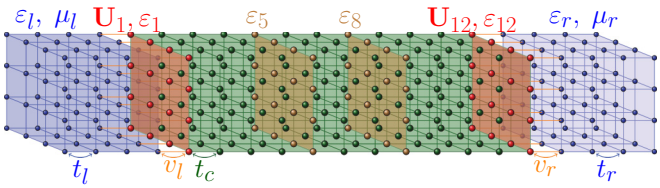

FIG. 1. Schematic representation of the triple-well system studied in this paper, consisting of a central region of 12 layers sandwiched between two semi-infinite metallic leads (blue), with chemical potentials $\mu_{l/r}$ and onsite energies $\varepsilon_{l/r} = \mu_{l/r}$, respectively. A Hubbard interaction is only present in the boundary layers (red, $z = 1,12$) with interaction strength $U_1 = U_{12} = U = 8$ and onsite energies $\varepsilon_1^{(0)} = \varepsilon_{12}^{(0)} = -U/2$. They form the outer walls of the quantum wells. The inner walls are the layers 5 and 8 (brown) and are caused by discontinuous onsite energies $\varepsilon_5^{(0)} = -\varepsilon_8^{(0)} = -4$, while all other layers have $\varepsilon_z^{(0)} = 0$. Energies are measured in units of the nearest-neighbor hopping t_c within the central region. For the nearest-neighbor hopping within the leads we use $t_l = t_r = 2$, and the hybridization between the left (right) lead and the central region is $v_l = v_r = 1$. A bias voltage $\Phi := \mu_l - \mu_r$ is applied to the leads, which linearly shifts the onsite energies of each layer: $\varepsilon_z = \varepsilon_z^{(0)} + \mu_l - z(\mu_l - \mu_r)/(L+1)$.

application of real-space dynamical mean-field theory within the nonequilibrium steady-state Green's function formalism for a system consisting of many layers. Afterwards, in Sec. IV, we present our results. Our conclusions are presented in Sec. V.

II. MODEL

The model, consisting of a central region (c) with $L = 12$ infinite and translationally invariant layers sandwiched between two semi-infinite metallic leads ($\alpha = l,r$), is described by the Hamiltonian (see Fig. 1):

$$\mathcal{H} = -\sum_{z,\langle \mathbf{r}_\perp,\mathbf{r}'_\perp\rangle_z,\sigma} t_z c^\dagger_{z,\mathbf{r}_\perp,\sigma} c_{z,\mathbf{r}'_\perp,\sigma} - \sum_{\langle z,z'\rangle,\mathbf{r}_\perp,\sigma} t_{zz'} c^\dagger_{z,\mathbf{r}_\perp,\sigma} c_{z',\mathbf{r}_\perp,\sigma} + \sum_{z,\mathbf{r}_\perp} U_z n_{z,\mathbf{r}_\perp,\uparrow} n_{z,\mathbf{r}_\perp,\downarrow} + \sum_{z,\mathbf{r}_\perp,\sigma} \varepsilon_z n_{z,\mathbf{r}_\perp,\sigma}, \quad (1)$$

with nearest-neighbor interlayer (intralayer) hopping $t_{zz'}$ (t_z), local onsite Hubbard interaction U_z and local energy ε_z. $\langle z,z'\rangle$ stands for neighboring z and z' layers and $\langle \mathbf{r}_\perp,\mathbf{r}'_\perp\rangle_z$ stands for neighboring $\mathbf{r}_\perp$ and $\mathbf{r}'_\perp$ sites of the zth layer. $c^\dagger_{z,\mathbf{r}_\perp,\sigma}$ creates an electron at site $\mathbf{r}_\perp$ of layer z with spin σ and $n_{z,\mathbf{r}_\perp,\sigma} = c^\dagger_{z,\mathbf{r}_\perp,\sigma} c_{z,\mathbf{r}_\perp,\sigma}$ denotes the corresponding occupation-number operator. $z = 1,\ldots,12$ describes the central layers, while $z < 1$ and $z > 12$ corresponds to the left and the right lead layers, respectively.

We assume isotropic nearest-neighbor hopping parameters within the central region ($t_{zz'} = t_z = t_c$) and within the leads ($t_{zz'} = t_z = t_{\alpha=l,r}$). The hybridization between the leads and central region is the same on both sides; $t_{0,1} = v_l = t_{12,13} = v_r$.

Finally, the local energy and the chemical potential in the leads is determined by an applied voltage Φ, i.e., $\varepsilon_{z<1} = \mu_l = \Phi/2$ and $\varepsilon_{z>12} = \mu_r = -\Phi/2$.

The leads are initially prepared in equilibrium and $T = 0$ at the distant past (time $\to -\infty$) when the hoppings between leads and layer are switched off. Then the hoppings are switched on and the system is allowed to evolve in time until steady state is reached. Notice that, despite the appearance of equilibrium Green's functions (7) in the expressions, there is no approximation of fixing the leads in equilibrium. In our approach, it is not necessary to solve explicitly for the transient time evolution, and we can directly address the steady state. Since the leads are infinite, they have equilibrium properties far away from the device, but near the device (within the healing length) there will be charge depletion or enhancement, i.e., charge reconstruction near the interfaces. In combination with the long-range part of the Coulomb interaction (LRCI) this could induce modifications in the single-particle potential. LRCI could be included by a simultaneous solution of the Poisson and DMFT equation (see, e.g., Ref. [49]), but this is beyond the scope of the present paper. Notice that this approximation is common in the framework of real-space DMFT calculations (see e.g., Refs. [34,35,45–48,75–78,80–85]). Here, we approximate the effects of the LRCI by introducing a linear behavior of the onsite energies (homogeneous electric field) in the central region as $\varepsilon_z = \varepsilon_z^{(0)} + \mu_l - z\Phi/(L+1)$.

III. REAL-SPACE DYNAMICAL MEAN-FIELD THEORY

To investigate steady-state properties we use real-space dynamical mean-field theory (R-DMFT), which is also known as inhomogeneous DMFT. Due to the finite number of layers, translational invariance along the z axes (perpendicular to the layers) is broken, but the system is still translationally invariant in the xy plane. Therefore we can introduce a corresponding momentum $\mathbf{k} = (k_x,k_y)$ [86].

The Green's function for the central region can be expressed via Dyson's equation

$$[\mathbf{G}^{-1}]^\gamma(\omega,\mathbf{k}) = \left[\mathbf{g}_0^{-1}(\omega,\mathbf{k})\right]^\gamma - \mathbf{\Sigma}^\gamma(\omega) - \mathbf{\Delta}^\gamma(\omega,\mathbf{k}). \quad (2)$$

Here, we use boldface symbols to indicate matrices in the indices $z = 1,\ldots,12$. Moreover, $\gamma \in \{R,A,K\}$ stands for retarded, advanced, and Keldysh components, respectively, and $\mathbf{G}^A(\omega,\mathbf{k}) = [\mathbf{G}^R(\omega,\mathbf{k})]^\dagger$.

The inverse of the noninteracting Green's function for the isolated central region reads

$$\left[\mathbf{g}_\mathbf{0}^{-1}\right]^R_{zz'}(\omega,\mathbf{k}) = \left[\omega + i0^+ - E_z(\mathbf{k})\right]\delta_{zz'} + t_{zz'}, \quad (3)$$

$$\left[\mathbf{g}_\mathbf{0}^{-1}\right]^K_{zz'}(\omega,\mathbf{k}) \simeq 0, \quad (4)$$

with $E_z(\mathbf{k}) = \varepsilon_z - 2t_z(\cos k_x + \cos k_y)$. $\mathbf{\Delta}^\gamma(\omega,\mathbf{k})$ describes the hybridization with the leads and can be expressed as

$$\mathbf{\Delta}^\gamma_{zz'}(\omega,\mathbf{k}) = \delta_{z,z'}\left[\delta_{z,1} v_l^2 g_l^\gamma(\omega,\mathbf{k}) + \delta_{z,L} v_r^2 g_r^\gamma(\omega,\mathbf{k})\right], \quad (5)$$

where $g_l^\gamma(\omega,\mathbf{k})$ and $g_r^\gamma(\omega,\mathbf{k})$ describe the Green's functions for the edge layers of the leads disconnected from the central region. Their retarded component can be expressed as [45,46,87]

$$g_\alpha^R(\omega,\mathbf{k}) = \frac{\omega - E_\alpha(\mathbf{k})}{2t_\alpha^2} - i\frac{\sqrt{4t_\alpha^2 - [\omega - E_\alpha(\mathbf{k})]^2}}{2t_\alpha^2}, \quad (6)$$

with $E_\alpha(\mathbf{k}) = \varepsilon_\alpha - 2t_\alpha(\cos k_x + \cos k_y)$. The sign of the square-root for negative argument must be chosen such that the Green's function has the correct $1/\omega$ behavior for $|\omega| \to \infty$. Since the disconnected leads are separately in equilibrium, we can obtain their Keldysh components from the retarded ones via the fluctuation dissipation theorem [88],

$$g^K_\alpha(\omega,\mathbf{k}) = 2i[1 - 2f_\alpha(\omega)]\mathrm{Im}\, g^R_\alpha(\omega,\mathbf{k}). \tag{7}$$

Here, $f_\alpha(\omega)$ is the Fermi distribution for chemical potential μ_α and temperature T_α.

Finally the self-energy $\mathbf{\Sigma}^\gamma_{zz'}(\omega) = \delta_{zz'}\Sigma^\gamma_z(\omega)$ is a diagonal and $\mathbf{k}$-independent matrix due to the DMFT approximation. To determine the self-energy for each correlated layer z we solve a (nonequilibrium) quantum impurity model with Hubbard interaction U_z and onsite energy ε_z, coupled to a self-consistently determined bath. The latter is specified by its hybridization function obtained as (see, e.g., Ref. [26])

$$\Delta^R_{\mathrm{bath},z}(\omega) = \omega + i0^+ - \varepsilon_z - \Sigma^R_z(\omega) - \frac{1}{G^R_{\mathrm{loc},z}(\omega)}, \tag{8}$$

$$\Delta^K_{\mathrm{bath},z}(\omega) = -\Sigma^K_z(\omega) + \frac{G^K_{\mathrm{loc},z}(\omega)}{|G^R_{\mathrm{loc},z}(\omega)|^2}, \tag{9}$$

where the local Green's function is defined as

$$G^\gamma_{\mathrm{loc},z}(\omega) = \int_{\mathrm{BZ}} \frac{d^2\mathbf{k}}{(2\pi)^2}\mathbf{G}^\gamma_{zz}(\omega,\mathbf{k}). \tag{10}$$

To calculate the diagonal elements of the matrices $\mathbf{G}^\gamma(\omega,\mathbf{k})$ one could invert the matrices in Eqs. (2). However, it is numerically more efficient to use the recursive Green's function method [76,89,90], which we here generalize to Keldysh Green's functions. For a given z we decompose the system into three decoupled clusters by setting $t_{z-1,z} = t_{z,z+1} = 0$ (for the first and the last layer into two decoupled clusters). The result is an isolated layer of the central region at position z and the two remaining parts of the central region to the left and to the right of layer z. By $L^\gamma_{z-1}(\omega,\mathbf{k})$ $[R^\gamma_{z+1}(\omega,\mathbf{k})]$ we denote the local Green's function at layer $z-1$ $(z+1)$ of the isolated cluster to the left (right) of layer z. In addition, we define $g^\gamma_z(\omega,\mathbf{k})$ as the full cluster Green's function of layer z [91]. For $z = 2,\ldots,L-1$ it describes isolated layers, while for $z = 1$ $(z = L)$ it also contains the hybridization effects of the left (right) lead, which are covered by $\Delta^\gamma(\omega,\mathbf{k})$. For the sake of better readability, we will suppress the argument $(\omega,\mathbf{k})$ in the following equations. From Eq. (2) and the ensuing definitions we readily see that the inverse cluster Green's function $[g^{-1}_z]^\gamma$ is equal to diagonal elements of the inverse $[\mathbf{G}^{-1}]^\gamma_{zz}$ of the full Green's function of the central region. The omitted hopping processes $t_{z-1,z}$ and $t_{z,z+1}$ can now be reintroduced by the Dyson equation, which is applicable due to the DMFT approximation of local self-energies. We obtain

$$\mathbf{G}^R_{zz} = \frac{1}{\left[g^{-1}_z\right]^R - t^2_{z-1,z}L^R_{z-1} - t^2_{z,z+1}R^R_{z+1}}, \tag{11}$$

$$\mathbf{G}^K_{zz} = -\frac{\left[g^{-1}_z\right]^K - t^2_{z-1,z}L^K_{z-1} - t^2_{z,z+1}R^K_{z+1}}{\left|[g^{-1}_z]^R - t^2_{z-1,z}L^R_{z-1} - t^2_{z,z+1}R^R_{z+1}\right|^2}. \tag{12}$$

The Green's functions L^γ_z and R^γ_z in turn are evaluated recursively as follows:

$$L^R_z = \frac{1}{\left[g^{-1}_z\right]^R - t^2_{z-1,z}L^R_{z-1}}, \tag{13}$$

$$L^K_z = -\frac{\left[g^{-1}_z\right]^K - t^2_{z-1,z}L^K_{z-1}}{\left|\left[g^{-1}_z\right]^R - t^2_{z-1,z}L^R_{z-1}\right|^2}, \tag{14}$$

for $z = 2,3,\ldots,L$ with initial values

$$L^R_1 = \frac{1}{\left[g^{-1}_1\right]^R}, \quad L^K_1 = -\frac{\left[g^{-1}_1\right]^K}{\left|\left[g^{-1}_1\right]^R\right|^2}, \tag{15}$$

and

$$R^R_z = \frac{1}{\left[g^{-1}_z\right]^R - t^2_{z,z+1}R^R_{z+1}}, \tag{16}$$

$$R^K_z = -\frac{\left[g^{-1}_z\right]^K - t^2_{z,z+1}R^K_{z+1}}{\left|\left[g^{-1}_z\right]^R - t^2_{z,z+1}R^R_{z+1}\right|^2}, \tag{17}$$

for $z = L-1, L-2,\ldots,1$ with initial values

$$R^R_L = \frac{1}{\left[g^{-1}_L\right]^R}, \quad R^K_L = -\frac{\left[g^{-1}_L\right]^K}{\left|\left[g^{-1}_L\right]^R\right|^2}. \tag{18}$$

In addition, the self-consistent DMFT loop works as follows: we start with an initial guess for the self-energies $\Sigma^\gamma_z(\omega)$, which typically was taken equal to zero, and based on Eqs. (2)–(10) we calculate the bath hybridization functions $\Delta^R_{\mathrm{bath},z}(\omega)$ and $\Delta^K_{\mathrm{bath},z}(\omega)$ for each correlated site. From them we solve the (nonequilibrium) quantum impurity models and calculate new self-energies as described below. We repeat this procedure until convergence is reached [92].

To address the impurity problem and evaluate self-energies, we adopt a recently developed auxiliary master equation approach (AMEA) [36,37,79]. This method can be seen as a generalization of the equilibrium exact-diagonalization impurity solver to treat nonequilibrium steady-state situations. In AMEA dissipation, which is crucial in order to achieve a steady state, is included by additionally coupling the cluster to Markovian environments, which can be seen as particle sinks and reservoirs (for details see Refs. [36,37,79,93]). The accuracy of the impurity solver increases with increase of N_b and becomes exponentially exact in the limit $N_b \to \infty$.

IV. RESULTS

Here, we presents results for the steady-state properties of the system, displayed in Fig. 1, consisting of twelve layers (central region) sandwiched between two semi-infinite metallic leads. Among these twelve central region layers only the first and the last layers are correlated, with Hubbard interactions $U_1 = U_{12} = U = 8$ and onsite energies $\varepsilon^{(0)}_1 = \varepsilon^{(0)}_{12} = -U/2 = -4$. The onsite energies of the fifth and the eight layers are $\varepsilon^{(0)}_8 = -\varepsilon^{(0)}_5 = 4$ and $\varepsilon^{(0)}_z = 0$ for all $z \neq 1,5,8,12$. The hopping between nearest-neighbor central region sites $t_c = 1$ is taken as unit of energy [94], while hopping between nearest-neighbor sites of the leads are $t_l = t_r = 2$. Finally, the hybridizations between leads and central

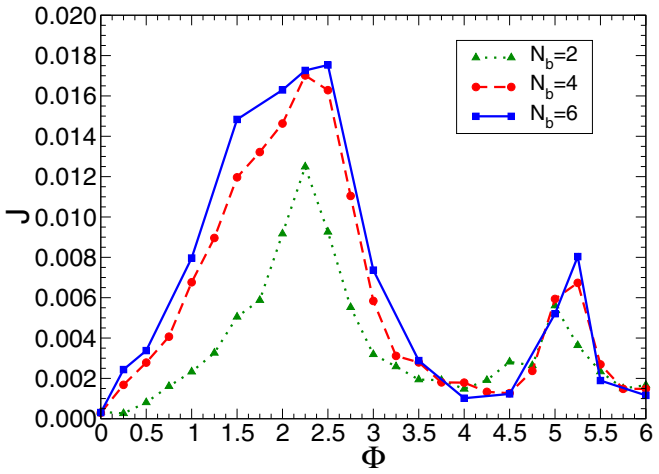

FIG. 2. Current J vs bias voltage Φ. Solid, dashed, and dotted lines are obtained by solving the impurity problem with $N_b = 6$, $N_b = 4$, and $N_b = 2$, respectively (see text). Parameters are the same as in Fig. 1.

region are $v_l = v_r = 1$. All calculations are performed for zero temperature in the leads ($T_l = T_r = 0$).

The system is particle-hole symmetric. More specifically, it is invariant under a simultaneous particle-hole transformation, a change of sign in the phase of one sublattice (as in the Hubbard model) together with a reflection of the z axis. Therefore, properties of layers z and $L + 1 - z$ are connected by particle-hole transformation. Consequently, we need to evaluate the self-energy for the $z = 1$ layer only and determine its value for $z = L$ layer based on the symmetry $[\Sigma^R_{12}(\omega) = -[\Sigma^R_1(-\omega)]^* + U$ and $\Sigma^K_{12}(\omega) = [\Sigma^K_1(-\omega)]^*]$. All other layers are noninteracting.

In Fig. 2 we plot the current-voltage characteristics of the system. Results are obtained with $N_b = 2,4,6$ bath sites of the DMFT auxiliary impurity problem. We find that the difference between results obtained with $N_b = 4$ and $N_b = 6$ is small for all bias voltages. It indicates fast convergence of the current with respect to the bath sites N_b.

The current increases with increasing bias voltage and reaches a first maximum at $\Phi \simeq 2.5$. Further increasing Φ reduces the current until a minimum at $\Phi \simeq 4$ is reached. A second maximum occurs at $\Phi \simeq 5.25$. For larger bias voltages, the current again decreases due to the decreased overlap of the density of states.

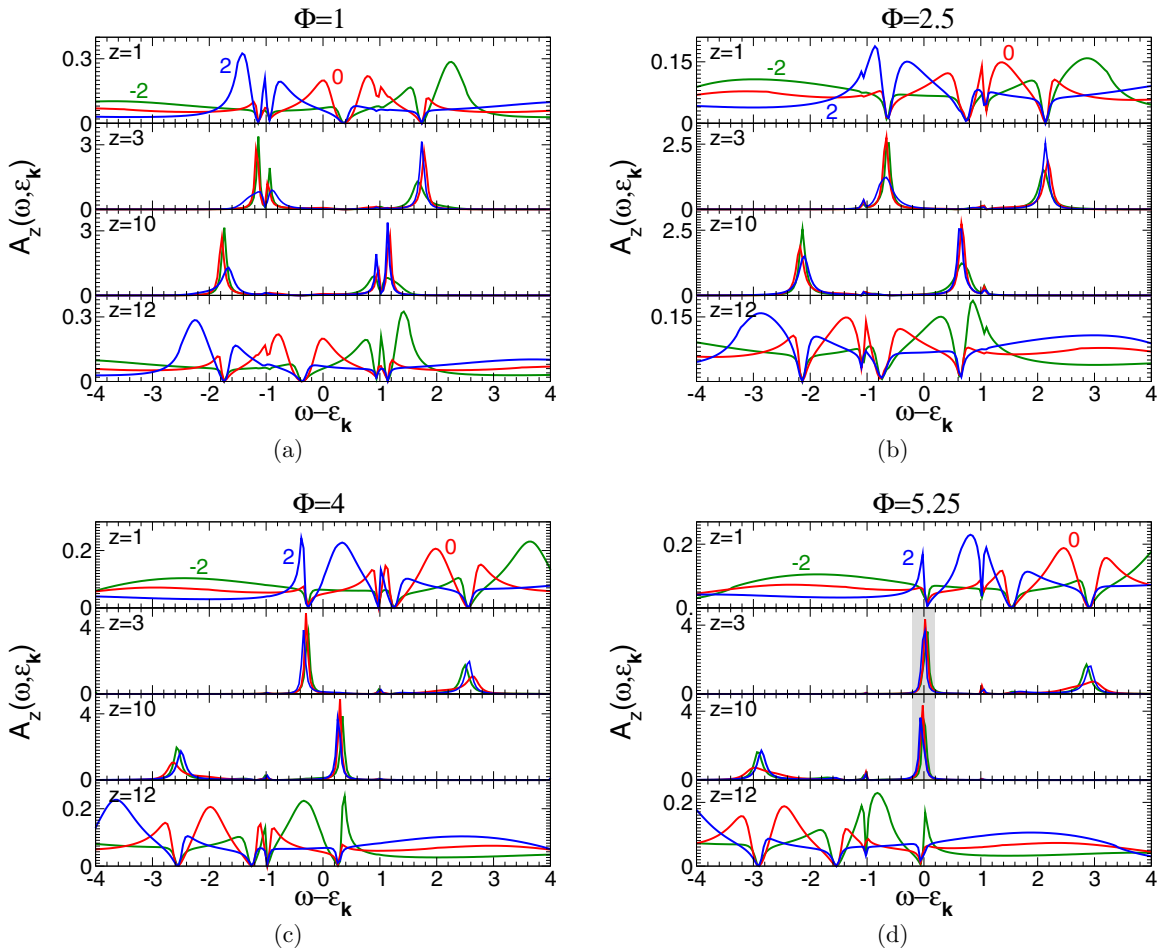

FIG. 3. Steady-state spectral function $A_z(\omega, \varepsilon_{\mathbf{k}})$ for different values of bias voltage Φ and $\varepsilon(\mathbf{k})$. To illustrate the resonance effect, we present results for bias voltages for which the current displays a maximum ($\Phi \simeq 2.5$ and $\Phi \simeq 5.25$), a minimum ($\Phi \simeq 4$), and for a value in between ($\Phi = 1$). The shaded area emphasizes the fact that, for $\Phi \simeq 5.25$, the peak maxima of layers $z = 3$ and $z = 10$ overlap. Results are obtained with $N_b = 6$. Here, $\varepsilon_{\mathbf{k}} = -2$ (green), $\varepsilon_{\mathbf{k}} = 0$ (red), and $\varepsilon_{\mathbf{k}} = 2$ (blue). Other parameters are the same as in Fig. 1.

For low bias, where there is a large overlap of the density of states of the left and the right leads, the conductivity is large and the system is in a high-conductivity regime. That is why results in this region are similar to the one of a single layer (see, e.g., Refs. [36,37]). In contrast, for larger bias $\Phi \gtrsim 3$ we are in the tunneling regime and the behavior of the current-voltage characteristics is significantly different. As we discuss below, the results we are showing are due to the occurrence of resonant tunneling. To clarify this effect, we investigate the nonequilibrium spectral functions, which can be calculated from the corresponding Green's functions via $A_z(\omega,\varepsilon_{\mathbf{k}}) = -\frac{1}{\pi}\mathrm{Im}G_z(\omega,\varepsilon_{\mathbf{k}})$. Due to the geometry of the system (see Fig. 1) three wells are formed in the intervals $2 \leqslant z \leqslant 4$, $6 \leqslant z \leqslant 7$, and $9 \leqslant z \leqslant 11$, to which electrons are partially confined and form quasibound levels. This can be seen by the fact that all spectral functions $A_z(\omega,\varepsilon_{\mathbf{k}})$ within a given well display peaks for the same $(\omega,\varepsilon_{\mathbf{k}})$, corresponding to quantized quasistationary levels in this well. Electrons can leak from the one to the next well only by quantum tunneling.

In Fig. 3 we plot the steady-state spectral functions $A_z(\omega,\varepsilon_{\mathbf{k}})$ as a function of $\omega - \varepsilon_{\mathbf{k}}$ for different $\varepsilon_{\mathbf{k}}$ and bias voltages Φ. In particular, we show results for bias voltages that correspond to maxima ($\Phi \simeq 2.5$ and $\Phi \simeq 5.25$), to a minimum and for a value ($\Phi = 1$) at half maximum of the first peak in Fig. 3.

The results have the correct property $A_{L+1-z}(\omega,\varepsilon_{\mathbf{k}}) = A_z(-\omega, -\varepsilon_{\mathbf{k}})$, which is a consequence of the particle-hole symmetry of the Hamiltonian. Our calculations show that, for each noncorrelated layer ($1 < z < 12$), the position of the peaks of the spectral function $A_z(\omega,\varepsilon_{\mathbf{k}})$ depends only on the value of $\omega - \varepsilon_{\mathbf{k}}$ and not on ω and $\varepsilon_{\mathbf{k}}$ separately. This indicates that, for the noncorrelated layers, one-dimensional physics dominates and $\varepsilon_{\mathbf{k}}$ only shifts the energy levels. Furthermore, peaks of the spectral functions $A_z(\omega,\varepsilon_{\mathbf{k}})$ for the noncorrelated layers in the first ($z = 2,3,4$) and the last ($z = 9,10,11$) wells generate dips in the spectral functions $A_z(\omega,\varepsilon_{\mathbf{k}})$ of the first ($z = 1$) and the last ($z = 12$) correlated layers correspondingly. This can be qualitatively understood from Eq. (11), if one assumes that $[\mathbf{G^{-1}}]^R_{zz}$ is a smooth function, while $-L^R_{z-1}$ or $-R^R_{z+1}$ (neighboring layer Green's functions) have narrow peaks.

Because central regions (layers $1 < z < 12$) are noninteracting, resonant tunneling occurs when quasistationary states, i.e., the peaks in the spectral function, of the first and the last well coincide for any $\varepsilon_{\mathbf{k}}$ [4,10]. This is the case for $\Phi \simeq 5.25$, as can be seen by the gray regions in Fig. 3(d). If these peaks are within the energetic transport window the current gets enhanced at the corresponding bias voltage. For all other bias voltages shown [see Figs. 3(a)–3(c)], peaks of $A_z(\omega,\varepsilon_{\mathbf{k}})$ for different wells do not coincide, so no resonant tunneling takes place. The second maximum in the current-voltage characteristics (see Fig. 2) can, therefore, be understood in terms of such a resonant tunneling effect. On the other hand, the first maximum is due to the finite bandwidth of the leads, similar to the one for a single-layer case (see, e.g., Refs. [36,37]). In contrast with the single-layer case, in the current situation electrons tunnel through four layers ($z = 1,5,8,12$) and therefore the current drops faster after the maximum.

To address the effect of electron correlation on the resonance, we investigate the behavior of the resonance current J as a function of the interaction U [95]. In Fig. 4 we plot the current

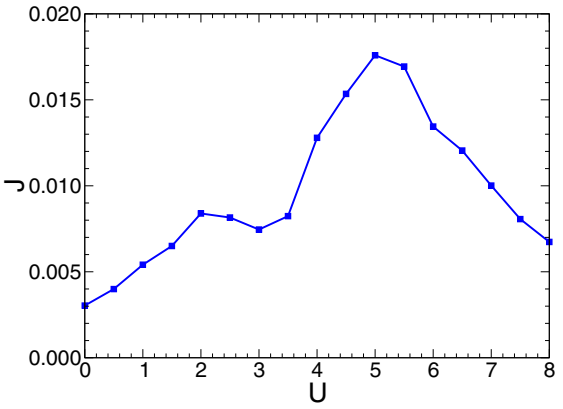

FIG. 4. Current J as a function of the Hubbard interaction U at the resonance. On-site energies in the first and the last layers are fixed to $\varepsilon^{(0)}_1 = \varepsilon^{(0)}_{12} = -4$. Results are obtained with $N_b = 4$. Other parameters are the same as in Fig. 1.

J as a function of the interaction U at the corresponding resonance bias voltage. The figure clearly shows that correlation effects substantially enhance the resonance effect. However, the current maximum is obtained at not too large values of $U \sim 5$. This enhancement behavior can be understood in terms of two competing effects occurring as a function of U: since the resonance takes place at relatively high bias, the *one-dimensional* density of states (DOS) of the two leads have a reduced overlap. This suppresses tunneling at small U for which scattering (approximately) conserves the momentum parallel to the layers. Upon increasing U, scattering channels to different values of the in-plane $\mathbf{k}$ open, so that the *three-dimensional* DOS is available for scattering, thus enhancing the current. On the other hand, by increasing U backscattering is also increased, which, in turns suppresses the current.

V. CONCLUSIONS

By using nonequilibrium DMFT calculations we investigate steady-state properties of a multilayer heterostructure consisting of correlated and noncorrelated layers. Due to the fact that the system is inhomogeneous, no matter how many impurity problems have to be solved, "standard" DMFT is not applicable and one has to use the real-space generalization of it. As an impurity solver we used the recently introduced auxiliary master equation approach, which addresses the impurity problem within an auxiliary system consisting of a correlated impurity, a small number of uncorrelated bath sites, and two Markovian environments described by a generalized master equation [36,37,79].

In particular, our main goal was to investigate resonance effects in this system. For this purpose we chose an arrangement of layers such that electrons were confined in three different wells and transport through the central region was only possible by quantum tunneling. For a particular bias voltage ($\Phi \simeq 5.25$) we observed that quasistationary energy levels in the first and the last wells coincided and resonance tunneling between them takes place. At that bias voltage the current displays a maximum. According to our calculations the current has another maximum at $\Phi \simeq 2.5$. The latter is due to the

finite bandwidth of the leads. We checked that these qualitative findings are robust up to some extent as a function of the model parameters.

Furthermore, we also investigate effect of the interaction strength on the current at the resonance. We obtain that correlation effects for weak up to strong interaction substantially enhance the resonance current.

ACKNOWLEDGMENTS

We thank Andreas Weichselbaum, Jim Freericks, Elias Assmann, and Max Sorantin for valuable discussions. This work was supported by the Austrian Science Fund (FWF): P26508, as well as by SFB-ViCoM project F04103 and NaWi Graz. The calculations were performed partly on the D-Cluster Graz and on the VSC-3 cluster Vienna.

[1] L. L. Chang, L. Esaki, and R. Tsu, Appl. Phys. Lett. **24**, 593 (1974).
[2] S. Datta, *Electronic Transport in Mesoscopic Systems* (Cambridge University Press, New York, 1995), Chaps. 2, 4, 5.
[3] S. Gurvitz, H. Lipkin, and Y. Prager, Phys. Lett. A **212**, 91 (1996).
[4] C. Ertler and W. Pötz, Phys. Rev. B **84**, 165309 (2011).
[5] F. Giazotto, P. Pingue, F. Beltram, M. Lazzarino, D. Orani, S. Rubini, and A. Franciosi, Phys. Rev. Lett. **87**, 216808 (2001).
[6] J. F. Rodriguez-Nieva, M. S. Dresselhaus, and L. S. Levitov, Phys. Rev. B **94**, 085412 (2016).
[7] A. F. Young and P. Kim, Nat. Phys. **5**, 222 (2009).
[8] T. L. M. Lane, J. R. Wallbank, and V. I. Fal'ko, Appl. Phys. Lett. **107**, 203506 (2015).
[9] R. M. Feenstra, D. Jena, and G. Gu, J. Appl. Phys. **111**, 043711 (2012).
[10] K. A. Guerrero-Becerra, A. Tomadin, and M. Polini, Phys. Rev. B **93**, 125417 (2016).
[11] B. Fallahazad, K. Lee, S. Kang, J. Xue, S. Larentis, C. Corbet, K. Kim, H. C. P. Movva, T. Taniguchi, K. Watanabe, L. F. Register, S. K. Banerjee, and E. Tutuc, Nano Lett. **15**, 428 (2015).
[12] S. Bruzzone, D. Logoteta, G. Fiori, and G. Iannaccone, Sci. Rep. **5**, 14519 (2015).
[13] S. C. de la Barrera and R. M. Feenstra, Appl. Phys. Lett. **106**, 093115 (2015).
[14] A. Mishchenko, J. S. Tu, Y. Cao, R. V. Gorbachev, J. R. Wallbank, M. T. Greenaway, V. E. Morozov, S. V. Morozov, M. J. Zhu, S. L. Wong, F. Withers, C. R. Woods, Y.-J. Kim, K. Watanabe, E. E. Taniguchi, T. Vdovin, O. Makarovsky, T. M. Fromhold, V. I. Fal'ko, L. Geim, A. K. Eaves, and K. S. Novoselov, Nat. Nanotechnol. **9**, 808 (2014).
[15] L. Brey, Phys. Rev. Appl. **2**, 014003 (2014).
[16] S. C. de la Barrera, Q. Gao, and R. M. Feenstra, J. Vac. Sci. Technol. B **32**, 04E101 (2014).
[17] A. A. Gorbatsevich and N. M. Shubin, arXiv:1608.04956.
[18] C. Presilla and J. Sjöstrand, J. Math. Phys. **37**, 4816 (1996).
[19] C. H. Ahn, S. Gariglio, P. Paruch, T. Tybell, L. Antognazza, and J.-M. Triscone, Science **284**, 1152 (1999).
[20] M. Izumi, Y. Ogimoto, Y. Konishi, T. Manako, M. Kawasaki, and Y. Tokura, Mater. Sci. Eng., B **84**, 53 (2001).
[21] S. Gariglio, C. H. Ahn, D. Matthey, and J.-M. Triscone, Phys. Rev. Lett. **88**, 067002 (2002).
[22] A. Ohtomo, D. A. Muller, J. L. Grazul, and H. Y. Hwang, Nature (London) **419**, 378 (2002).
[23] A. Ohtomo and H. Y. Hwang, Nature (London) **427**, 423 (2004).
[24] Q. X. Zhu, W. Wang, X. Q. Zhao, X. M. Li, Y. Wang, H. S. Luo, H. L. W. Chan, and R. K. Zheng, J. Appl. Phys. **111**, 103702 (2012).
[25] A. Georges, G. Kotliar, W. Krauth, and M. J. Rozenberg, Rev. Mod. Phys. **68**, 13 (1996).
[26] D. Vollhardt, in *Lecture Notes on the Physics of Strongly Correlated Systems*, Vol. 1297, edited by A. Avella and F. Mancini (AIP, New York, 2010), pp. 339–403.
[27] W. Metzner and D. Vollhardt, Phys. Rev. Lett. **62**, 324 (1989).
[28] H. Aoki, N. Tsuji, M. Eckstein, M. Kollar, T. Oka, and P. Werner, Rev. Mod. Phys. **86**, 779 (2014).
[29] P. Schmidt and H. Monien, arXiv:cond-mat/0202046.
[30] J. K. Freericks, V. M. Turkowski, and V. Zlatić, Phys. Rev. Lett. **97**, 266408 (2006).
[31] J. K. Freericks, Phys. Rev. B **77**, 075109 (2008).
[32] A. V. Joura, J. K. Freericks, and T. Pruschke, Phys. Rev. Lett. **101**, 196401 (2008).
[33] M. Eckstein, M. Kollar, and P. Werner, Phys. Rev. Lett. **103**, 056403 (2009).
[34] S. Okamoto, Phys. Rev. B **76**, 035105 (2007).
[35] S. Okamoto, Phys. Rev. Lett. **101**, 116807 (2008).
[36] E. Arrigoni, M. Knap, and W. von der Linden, Phys. Rev. Lett. **110**, 086403 (2013).
[37] I. Titvinidze, A. Dorda, W. von der Linden, and E. Arrigoni, Phys. Rev. B **92**, 245125 (2015).
[38] A. Dorda, I. Titvinidze, and E. Arrigoni, J. Phys.: Conf. Ser. **696**, 012003 (2016).
[39] R. Kubo, J. Phys. Soc. Jpn. **12**, 570 (1957).
[40] J. Schwinger, J. Math. Phys. **2**, 407 (1961).
[41] G. Baym and L. P. Kadanoff, Phys. Rev. **124**, 287 (1961).
[42] L. P. Kadanoff and G. Baym, *Quantum Statistical Mechanics: Green's Function Methods in Equilibrium and Nonequilibrium Problems* (Addison-Wesley, Redwood City, 1962).
[43] L. V. Keldysh, Zh. Eksp. Teor. Fiz. **47**, 1515 (1965) [JETP **20**, 1018 (1965)].
[44] P. W. Anderson, Phys. Rev. **124**, 41 (1961).
[45] M. Potthoff and W. Nolting, Phys. Rev. B **59**, 2549 (1999).
[46] M. Potthoff and W. Nolting, Phys. Rev. B **60**, 7834 (1999).
[47] M. Potthoff and W. Nolting, Eur. Phys. J. B **8**, 555 (1999).
[48] M. Potthoff and W. Nolting, Physica B (Amsterdam, Neth.) **259-261**, 760 (1999).
[49] J. K. Freericks, *Transport in Multilayered Nanostructures* (Imperial College Press, London, 2006).
[50] R. Nourafkan, F. Marsiglio, and M. Capone, Phys. Rev. B **82**, 115127 (2010).
[51] H. Ishida and A. Liebsch, Phys. Rev. B **79**, 045130 (2009).
[52] R. Nourafkan and F. Marsiglio, Phys. Rev. B **83**, 155116 (2011).
[53] S. Okamoto, Phys. Rev. B **84**, 201305 (2011).
[54] P. Miller and J. K. Freericks, J. Phys.: Condens. Matter **13**, 3187 (2001).
[55] J. K. Freericks, Phys. Rev. B **70**, 195342 (2004).

[56] S. Okamoto and A. J. Millis, Phys. Rev. B **70**, 241104 (2004).
[57] V. Dobrosavljević and G. Kotliar, Phys. Rev. Lett. **78**, 3943 (1997).
[58] V. Dobrosavljević and G. Kotliar, Philos. Trans. R. Soc., A **356**, 57 (1998).
[59] Y. Song, R. Wortis, and W. A. Atkinson, Phys. Rev. B **77**, 054202 (2008).
[60] J. Wernsdorfer, G. Harder, U. Schollwoeck, and W. Hofstetter, arXiv:1108.6057.
[61] R. W. Helmes, T. A. Costi, and A. Rosch, Phys. Rev. Lett. **100**, 056403 (2008).
[62] A. Koga, T. Higashiyama, K. Inaba, S. Suga, and N. Kawakami, J. Phys. Soc. Jpn. **77**, 073602 (2008).
[63] A. Koga, T. Higashiyama, K. Inaba, S. Suga, and N. Kawakami, Phys. Rev. A **79**, 013607 (2009).
[64] K. Noda, A. Koga, N. Kawakami, and T. Pruschke, Phys. Rev. A **80**, 063622 (2009).
[65] A. Koga, J. Bauer, P. Werner, and T. Pruschke, Physica E (Amsterdam, Neth.) **43**, 697 (2011).
[66] N. Blümer and E. Gorelik, Comput. Phys. Commun. **182**, 115 (2011).
[67] D.-H. Kim, J. J. Kinnunen, J.-P. Martikainen, and P. Törmä, Phys. Rev. Lett. **106**, 095301 (2011).
[68] M. W. Aulbach, F. F. Assaad, and M. Potthoff, Phys. Rev. B **92**, 235131 (2015).
[69] M. Snoek, I. Titvinidze, C. Take, K. Byczuk, and W. Hofstetter, New J. Phys. **10**, 093008 (2008).
[70] M. Snoek, I. Titvinidze, and W. Hofstetter, Phys. Rev. B **83**, 054419 (2011).
[71] I. Titvinidze, A. Schwabe, N. Rother, and M. Potthoff, Phys. Rev. B **86**, 075141 (2012).
[72] E. V. Gorelik, I. Titvinidze, W. Hofstetter, M. Snoek, and N. Blümer, Phys. Rev. Lett. **105**, 065301 (2010).
[73] A. Schwabe, I. Titvinidze, and M. Potthoff, Phys. Rev. B **88**, 121107 (2013).
[74] M. W. Aulbach, I. Titvinidze, and M. Potthoff, Phys. Rev. B **91**, 174420 (2015).
[75] H. Zenia, J. K. Freericks, H. R. Krishnamurthy, and T. Pruschke, Phys. Rev. Lett. **103**, 116402 (2009).
[76] M. Eckstein and P. Werner, Phys. Rev. B **88**, 075135 (2013).
[77] M. Eckstein and P. Werner, Phys. Rev. Lett. **113**, 076405 (2014).
[78] S. T. F. Hale and J. K. Freericks, Phys. Rev. B **83**, 035102 (2011).
[79] A. Dorda, M. Nuss, W. von der Linden, and E. Arrigoni, Phys. Rev. B **89**, 165105 (2014).
[80] M. Knap, W. von der Linden, and E. Arrigoni, Phys. Rev. B **84**, 115145 (2011).
[81] J. Neumayer, E. Arrigoni, M. Aichhorn, and W. von der Linden, Phys. Rev. B **92**, 125149 (2015).
[82] G. Mazza, A. Amaricci, M. Capone, and M. Fabrizio, Phys. Rev. B **91**, 195124 (2015).
[83] G. Mazza, A. Amaricci, M. Capone, and M. Fabrizio, Phys. Rev. Lett. **117**, 176401 (2016).
[84] A. Amaricci, C. Weber, M. Capone, and G. Kotliar, Phys. Rev. B **86**, 085110 (2012).
[85] P. Ribeiro, A. E. Antipov, and A. N. Rubtsov, Phys. Rev. B **93**, 144305 (2016).
[86] For a treatment of a similar nonequilibrium system by R-DMFT see also [35]. There a NCA impurity solver was used.
[87] R. Haydock, *Solid State Physics, Advances in Research and Applications*, edited by H. Ehrenreich, F. Seitz, and D. Turnbull (Academic, London, 1980), Vol. 35.
[88] H. Haug and A.-P. Jauho, *Quantum Kinetics in Transport and Optics of Semiconductors* (Springer, Heidelberg, 1998).
[89] D. J. Thouless and S. Kirkpatrick, J. Phys. C: Solid State Phys. **14**, 235 (1981).
[90] C. H. Lewenkopf and E. R. Mucciolo, J. Comput. Electron. **12**, 203 (2013).
[91] For the Keldish Green's function holds the following relation $g_z^K = -[g_z^{-1}]^K/|g_z^R|^2$.
[92] We compare two consecutive hybridization functions in the DMFT iteration and use as convergence criterion that the root-mean-square deviation $\sqrt{\int d\omega(|\Delta^R_{\rm new}(\omega) - \Delta^R_{\rm old}(\omega)|^2 + |\Delta^K_{\rm new}(\omega) - \Delta^K_{\rm old}(\omega)|^2)} < 10^{-6}$. Here we also note that $\int d\omega|\Delta^\gamma(\omega)| > 1$.
[93] A. Dorda, M. Ganahl, H. G. Evertz, W. von der Linden, and E. Arrigoni, Phys. Rev. B **92**, 125145 (2015).
[94] Usually, hopping t_c is of the order of 1 eV.
[95] These results are obtained by fixing a potential barrier $\varepsilon_1^{(0)} = \varepsilon_{12}^{(0)} = -4$ for all U values, otherwise there would be no barrier at $U = 0$.